Low Temperature Physics

Raman scattering under structural and magnetic phase transitions in terbium ferroborate

Cite as: Low Temp. Phys. **40**, 171 (2014); https://doi.org/10.1063/1.4865566
Published Online: 03 March 2014

A. V. Peschanskii, A. V. Yeremenko, V. I. Fomin, L. N. Bezmaternykh, and I. A. Gudim

View Online Export Citation CrossMark

ARTICLES YOU MAY BE INTERESTED IN

Raman scattering in multiferroic $SmFe_3(BO_3)_4$
Low Temperature Physics **42**, 475 (2016); https://doi.org/10.1063/1.4954783

Spin-phonon coupling in antiferromagnetic nickel oxide
Applied Physics Letters **111**, 252402 (2017); https://doi.org/10.1063/1.5009598

$BaTiO_3$-based piezoelectrics: Fundamentals, current status, and perspectives
Applied Physics Reviews **4**, 041305 (2017); https://doi.org/10.1063/1.4990046

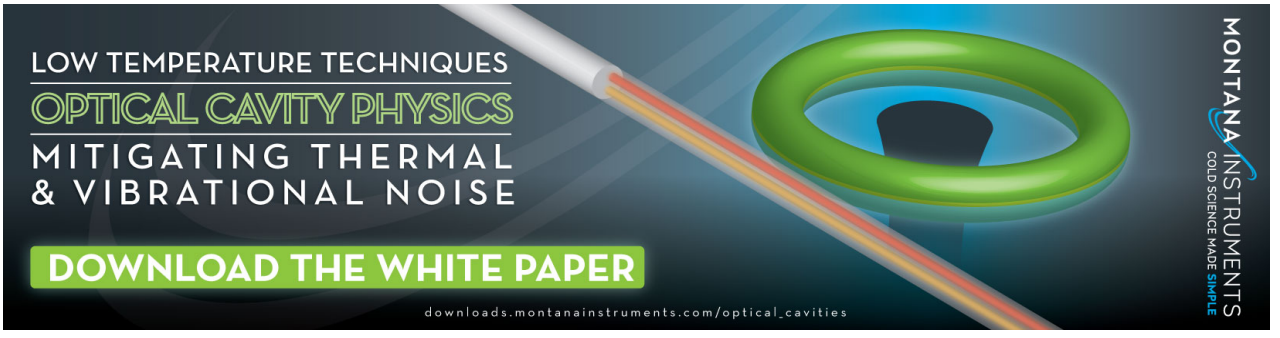

AIP Publishing

© 2014 AIP Publishing LLC.

Raman scattering under structural and magnetic phase transitions in terbium ferroborate

A. V. Peschanskii,[a] A. V. Yeremenko, and V. I. Fomin

B. I. Verkin Institute for Low Temperature Physics and Engineering of the National Academy of Sciences of Ukraine, 47 Lenin Ave., Kharkov 61103, Ukraine

L. N. Bezmaternykh and I. A. Gudim

L. V. Kirenskii Institute of Physics, Siberian Branch of the Russian Academy of Sciences, Krasnoyarsk 660036, Russia

(Submitted August 12, 2013)
Fiz. Nizk. Temp. **40**, 219–229 (February 2014)

The Raman scattering spectrum of single crystal $TbFe_3(BO_3)_4$ was studied in the frequency range 3–500 cm^{-1} at temperatures from 2 to 300 K. It was found that in high- and low-temperature phases there exist additional phonon lines which were not known before. In the high-temperature phase, these lines originate from LO–TO splitting of polar phonons. Appearance of the additional lines in the low temperature phase is due to both a reduction of the crystal symmetry under the phase transition and an increase of the primitive cell volume. It was established that the frequencies of some phonon lines in the magneto-ordered phase are shifted towards the high-energy region upon applying an external magnetic field along the third-order axis. The spectrum of two-magnon Raman scattering was investigated. It was shown that at low temperatures the two-magnon band has a complex shape that reflects specific features in the density of state of the magnon branches. The magnon energy at the Brillouin zone boundary was determined. © *2014 AIP Publishing LLC*.
[http://dx.doi.org/10.1063/1.4865566]

Introduction

Recently, in connection with the discovery of the magnetoelectric effect in $GdFe_3(BO_3)_4$,[1,2] $NdFe_3(BO_3)_4$,[3] $HoFe_3(BO_3)_4$[4] and $SmFe_3(BO_3)_4$[5] compounds, a new class of materials, rare-earth ferroborates $ReFe_3(BO_3)_4$, is intensively studied. Integrated studies of magnetic, magnetoelectric and magnetoelastic properties of $ReFe_3(BO_3)_4$ compounds showed a significant dependence of these properties on the type of the rare-earth ion Re.[6] Most of $ReFe_3(BO_3)_4$ compounds exhibit a structural phase transition (PT) with a reduction in symmetry. Iron spins in ferroborates are strongly correlated and antiferromagnetically ordered below a temperature of ~30–40 K. The complexity of the magnetic interactions in these systems due to the presence of two different types of magnetic ions (3*d*- and 4*f*-elements) complicates understanding of their magnetoelectric properties. The nature of the relation between the magnetic and ferroelectric ordering in rare-earth ferroborates is currently intensively discussed.

Terbium ferroborate $TbFe_3(BO_3)_4$ crystallizes in the space group $R32$ ($z = 1$). The main structural motif is the helical chains directed along the trigonal *c*-axis and composed of the connected by an edge FeO_6 octahedra, which include Fe^{3+} ions. $TbFe_3(BO_3)_4$ undergoes a first-order structural phase transition at $T_s = 192$ K.[7] Spatial symmetry group change upon the transition $R32$ ($z = 1$) → $P3_121$ ($z = 3$) means that the crystal class 32 remains unchanged, however there is a "loss" of certain spatial translations.[7] Volume of the new hexagonal primitive cell triples. However, more recent X-ray studies revealed a very weak structural deviations from the space group $P3_121$ ($z = 3$) at $T < T_s$ in Y, Gd, and Tb ferroborates.[8]

Below the Neel temperature $T_N = 40$ K, terbium ferroborates becomes a uniaxial antiferromagnet (AFM) with the spins of Fe^{3+} ions oriented along the trigonal axis. Structural and magnetic phase transitions are accompanied by a highly anisotropic thermal expansion as well as by anomalies of dielectric properties.[7,9]

The temperature dependences of the real part of dielectric constants ε_c and ε_{ab} exhibit jumps at T_s. Upon lowering temperature below T_s, the dependences $\varepsilon_c(T)$ and $\varepsilon_{ab}(T)$ become decreasing functions of temperature. Measurement at 1 kHz showed that lowering temperature below $T_N \approx 39$ K leads to an additional slight decrease in ε_c. Upon lowering temperature, ε_{ab} decreases from ~37.2 to ~34.8 with a jump of ~1.2 at T_s. The dependence ε_{ab}(T) exhibits a minimum in the paramagnetic region at approximately 50 K, below which there is a slight increase with a broad maximum at 20 K.[9] Measurements of the dielectric constant in the submillimeter wavelength range (2–16 cm^{-1}) showed a similar pattern of changes in ε_c and ε_{ab}.[10] At a frequency of 390 GHz, which is lower than the frequency of the AFM resonance (~14.9 cm^{-1} at 6.6 K), the most noticeable jump at T_s is observed in $\varepsilon_c(T)$. However, ε_{ab} only slightly varies with temperature, lies in the range $14.4 > \varepsilon_{ab} > 12.2$, and exhibits a small jump at the structural transition. No frequency dependence of the permittivity at frequencies from 60 to 480 GHz (2–16 cm^{-1}) has been detected. A big difference in the values of ε_{ab} over the entire temperature range as well as in the magnitude of the jump at T_s as compared with the measurements at 1 kHz should be noted.[9]

Upon applying a magnetic field $\mathbf{H} \parallel c$, a spin-flop transition ($H_{sf} = 35$ kOe at 4.2 K) at which the spins of Fe^{3+} fall into the basal plane *ab* is observed. This magnetic-field-induced transition is characterized by a large jump in magnetization as well as the appearance of electric polarization and magnetoelastic deformations.[6] The magnitude of the electric polarization jumps ΔP at H_{sf} is small.

 © 2014 AIP Publishing LLC

The microscopic nature of the magnetoelectric coupling in rare ferroborates is still being debated. The emergence of the electric dipole moment is reflected in the spectrum of polar lattice vibrations. The Lyddane-Sachs-Teller relation couples the dielectric constants ε_0 and ε_∞ and the frequencies of long-wavelength longitudinal (LO) and transverse (TO) optical modes: $\varepsilon_0 = \varepsilon_\infty(\omega_{LO}/\omega_{TO})^2$. The dielectric constant ε_{ab} is determined by the contribution of polar vibrational modes propagating perpendicular to the c-axis of the crystal. Studies of the IR reflectance spectrum of crystal $TbFe_3(BO_3)_4$ in the polarization $\mathbf{E} \perp c$ and the frequency range 200–2000 cm^{-1} have shown that the spectrum contains both broad intense and sufficiently narrow weak bands.[11] However, the spectrum shows no significant change when the temperature is lowered to 10 K. The influence of the magnetic ordering at $T_N = 40$ K has also not been revealed.

Inelastic light scattering spectra of several $ReFe_3(BO_3)_4$ crystals (Re = Gd, Nd, Tb, Er, and Y) have been studied in a wide temperature range including a variety of structural and magnetic phases.[12–14] It has been shown that vibrational excitations with the energies below about 500 cm^{-1} can be considered as external vibrational modes of the crystal lattice.

The magnetic subsystem in terbium ferroborate consists of iron and terbium ions. Strong spin-orbit coupling in terbium ions leads to significant magnetic anisotropy of the easy-axis type directed along the c-axis of the crystal. Different interaction mechanisms between the magnetic and phonon subsystems have been examined. The influence of magnetoelastic interaction on single-ion magnetic anisotropy of terbium ions has been considered theoretically in Ref. 15. However, results of an experimental study of the acoustic characteristics of $TbFe_3(BO_3)_4$ have shown that, apparently, the coupling with single-ion magnetic anisotropy does not constitute the main mechanism.[16] Another explanation for the discrepancy between theory and experiment can be that it is not acoustic but optical vibrations that are coupled to single-ion anisotropy.[16]

The important role of optical vibrational modes follows from experimental studies of magnetoelastic and magnetodielectric coupling in terbium ferroborate.[9] Measurements of the dielectric constants and magnetostriction have shown that the magnetoelectric coupling cannot be explained by the magnetostriction effect. The coupling occurs as a result of the frequency shift of certain transverse optical vibrational modes. A smooth decrease of ε_{ab} in the temperature range $T_s > T > T_N$ results from the contributions of all TO modes propagating in the ab-plane, however the most effective contribution, according to the authors of Ref. 9, is due to 200 cm^{-1} mode. It has been found that when the temperature is lowered below T_N, only two low-frequency modes, 200 and 260 cm^{-1}, of the vibrational spectrum of $TbRe_3(BO_3)_4$ experience a noticeable frequency shift.[9] According to the authors, a softening of E-mode with frequency $\omega_{E(TO)} \sim 200\ cm^{-1}$ may be the cause of the anomalous behavior of the dielectric constant ε_{ab} at $T < T_N$.

Detailed studies of polar excitations in $TbFe_3(BO_3)_4$ can reveal the nature of the changes in the dielectric properties under the structural phase transition as well as under the magnetic ordering. In addition, some aspects related to the manifestation of the magnetic ordering in the spectra of low-energy excitations (in the range which includes spin-wave frequencies) have not been fully elucidated. This paper presents the results of the study of Raman scattering in terbium ferroborate in the frequency range 3–500 cm^{-1} at temperatures 2–300 K. The main focus of the study was on the temperature behavior of the polar E-modes 200 and 260 cm^{-1} and the low-energy (5–180 cm^{-1}) excitation spectrum. In the antiferromagnetically ordered state (at $T = 5$ K), their behavior was studied in magnetic fields up to 30 kOe applied along and perpendicular to the trigonal c-axis of crystal $TbFe_3(BO_3)_4$.

Samples and measurement techniques

Measurements were carried out on a $TbFe_3(BO_3)_4$ crystal of good optical quality, grown from a solution-melt based on bismuth trimolibdate following the procedure described in Ref. 17. The sample was cut in the shape of a rectangular parallelepiped, 2.2 × 2.7 × 4.8 mm, with carefully polished faces. Its edges were aligned parallel to the axes $Z \parallel C_3$, $X \parallel C_2$, and $Y \perp Z, X$. Orientation was performed using the x-ray method. The sample quality was checked with a polarizing microscope. Orientation of the C_3-axis was maintained with an accuracy of 1°.

Raman studies were performed in the 90° configuration. The scattering was excited with a HeNe laser at $\lambda = 632.8$ nm (30 mW) and a solid-state laser at $\lambda = 532$ nm (35 and 100 mW). The scattered light was analyzed with a double monochromator Ramanor U-1000 and detected using a cooled photomultiplier RCA 31034 and a photon counting circuit. In optical cryostats, the sample was immersed in helium vapor, which allowed both to study temperature dependences and perform measurements at 5 K in a magnetic field up to 30 kOe produced by a superconducting solenoid.

Raman scattering spectra are presented in the standard notation $k(ij)q$, where k and q are the propagation directions of the incident and scattered light with the electric vector **e** pointing along the i and j directions, respectively. Notations ZZ, XY, etc. correspond to the specific components of the scattering tensor.

Group-theoretical analysis of the vibrational excitation in $TbFe_3(BO_3)_4$

Group-theoretical analysis of the vibrational excitations in rare-earth ferroborates has been presented in Ref. 12. The number and symmetry of the lattice vibrations in different structural phases are given below.

Structure R32 (D_3^7)

The primitive cell contains one formula unit. The lattice vibrations are described by $\Gamma_{vibr} = 7A_1 + 13A_2 + 20E$ symmetry types, out of which $\Gamma_{ac} = A_2 + E$ are the acoustic ones. A_1- and doubly degenerated E-modes are active in Raman scattering. Nonzero components of the scattering tensor in the above configuration have the form: A_1: XX, YY, and ZZ; $E(x)$: XX, YY, YZ, and ZY; $E(y)$: XY, YX, XZ, and ZX.[18] The polarization vector of E-phonons (shown in brackets) lies in the ab-plane with the wave vector **k** in the XY-plane for TO + LO phonons and along the Z-axis for TO phonons. The frequency range of 3–500 cm^{-1} contains $3A_1 + 8A_2 + 11E$ optical modes.[12]

Structure $P3_121$ (D_3^4)

It is assumed that the structural distortions found in Ref. 8 are small and the primitive cell of the low-temperature structure contains three formula units. The lattice vibrations include $\Gamma_{vibr} = 27A_1 + 32A_2 + 59E$ optical modes, out of which $15A_1 + 20A_2 + 35E$ are expected to be present in the frequency range under study.

A_1- and E-modes are active in Raman scattering in both the high- and low-temperature phases.[18]

Experimental results

Fig. 1 shows the polarized Raman spectra in the region of the external vibrational modes at room temperature excited at $\lambda = 632.8$ nm. In this experimental geometry, the spectrum with a ZZ-component of the scattering tensor is observed. Since the spectra with XX- and YY-components contain both A_1- and E-modes, this allows to uniquely identify A_1-modes. As follows from the group-theoretical analysis, $3A_1$-nonpolar modes are observed (Fig. 1). A greater number of lines than expected in this range were observed in the spectra with off-diagonal components of the scattering tensor (E-modes). This is due to the splitting of the E-modes into TO and LO components, which are simultaneously observed in the spectra in the present scattering geometry.

In order to separate TO and LO components, different sample arrangements were used in which phonons propagate at an angle $\theta = 45°$ to the third-order axis, but only either LO or TO component in the spectra is observed. As an example, Fig. 2 shows the Raman spectra at room temperature with YY- and in three geometries with XY-components of the scattering tensor. A solid-state laser with $\lambda = 532$ nm was utilized for these measurements. The spectra were similar (in terms of the number of lines, their width and intensity ratio) to those obtained at $\lambda = 632.8$ nm. The spectral resolution deteriorates when a laser at $\lambda = 532$ nm is used, however this is not essential for the room temperature spectra since the half-width of the observed lines exceeds the instrumental function. Moreover, the quality of the spectra increases and, when the spectra are decomposed into a sum of Lorentzians, the accuracy of determination of the line parameters improves. As already noted, in the spectra with $\theta = 90°$, both TO and LO components were observed. The lines of those

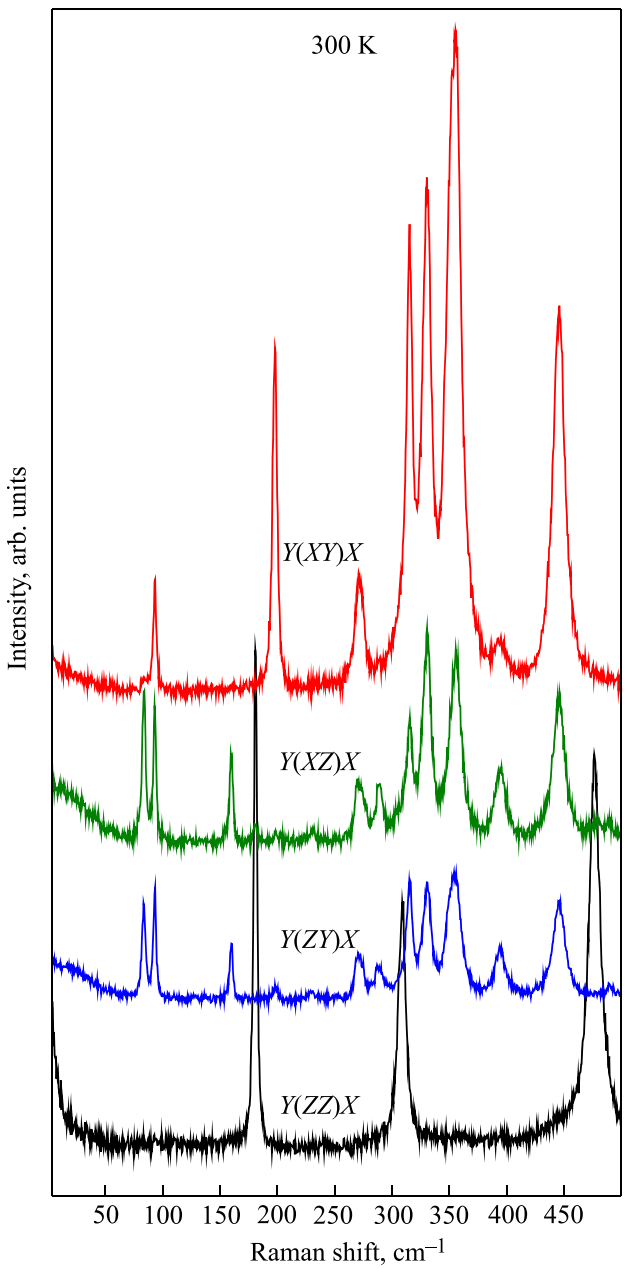

FIG. 1. Raman spectra with different polarizations in the region of external vibrational modes of single crystal $TbFe_3(BO_3)_4$ at 300 K. The excitation line $\lambda_{exc} = 632.8$ nm (30 mW). The spectral resolution is 1.8 cm^{-1}.

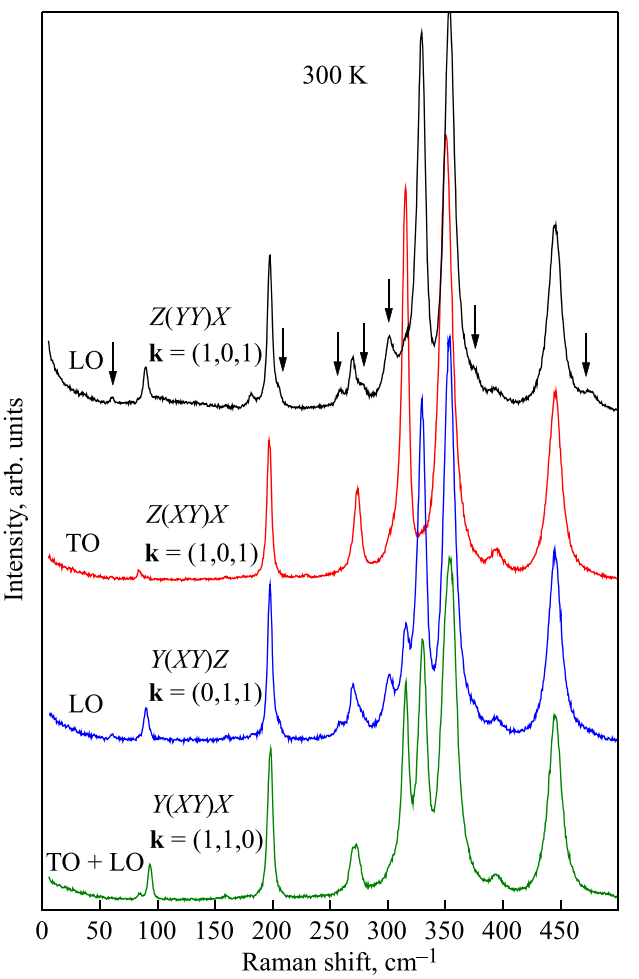

FIG. 2. Raman spectra of single crystal $TbFe_3(BO_3)_4$ observed in various geometries with YY-and XY-components of the scattering tensor at 300 K; $\lambda_{exc} = 532$ nm (35 mW). The spectral resolution is 3.0 cm^{-1}.

TABLE 1. Energy (in cm^{-1}) of the vibrational modes observed in single crystal $TbFe_3(BO_3)_4$ at 300 K in comparison with literature data. The energy at 2K is shown in brackets.

$TbFe_3(BO_3)_4$, present study, 300 K (2 K)					$TbFe_3(BO_3)_4$, Ref. 12		$GdFe_3(BO_3)_4$, Ref. 12		
A_1	E_{TO}	E_{LO}	E_{LO} ($\theta=45°$)	A_2 ($\theta=45°$)	A_1	E	A_1	E_{TO}	E_{LO}
180.6 (182.4)	84.2(89.1)	93.6 (97.0)	89.5	60.5	180	93	180	84	93
308.2 (310.4)	159.9 (158.5)		–	205.4	309	159	307	160	160
476.0 (474.5)	197.1 (199.0)	198.3 (199.8)	197.6	258.5	476	198	475	195	198
–	230.4 (235.0)		–	277.2	–	230	–	–	232
–	269.4 (274.0)		–	301.4	–	270	–	270	270
–	273.5 (278.1)	289.0 (291.3)	–	372.6	–	287	–	273	287
–	315.4 (318.4)	330.4 (332.1)	329.4	470.0	–	330	–	315	330
–	350.7 (349.3)	355.8 (351.5)	353.4	–	–	355	–	352	357
–	394.2 (403.5)		–	–	–	392	–	391	391
–	445.0 (450.3)		–	–	–	444	–	443	443
–	489.0 (492.0)		–	–	–	480	–	–	488

spectra which had a small TO-LO splitting (regions ~200 and ~350 cm^{-1}) were described as a sum of two lines. During the processing, the parameters of the TO-component line taken from the spectra corresponding only to TO were fixed, while the parameters of the line corresponding to LO component were varied. Results of such treatment, the energies of the observed vibrational modes, are shown in Table 1. It also shows literature data for $TbFe_3(BO_3)_4$ and isostructural $GdFe_3(BO_3)_4$ crystals.[12] As seen from Table 1, $3A_1 + 11E$ vibrational modes expected in this range were observed. The splitting of several lines into TO and LO components has similar values to that observed for the crystal $GdFe_3(BO_3)_4$.[12]

In addition to these $3A_1 + 11E$ vibrational modes, at $\theta = 45°$ in the spectra corresponding to the LO components, there were observed several weak lines indicated by arrows in Fig. 2. Their frequencies are shown in Table 1 at $\theta = 45°$. They are assigned to polar A_2 modes, which are forbidden by selection rules in inelastic scattering at $\theta = 0°$ and $\theta = 90°$. Possibility to observe inactive A_2 polar excitations at $\theta = 45°$ due to their interaction with active E-modes has been demonstrated for α-quartz.[19,20]

Fig. 3 shows polarized Raman spectra of the $TbFe_3(BO_3)_4$ crystal in the region of external vibrational modes in the low-temperature phase at 2 K. As can be seen from a comparison with Fig. 1, a large number of additional lines and a broad band at ~74 cm^{-1} are observed in the spectra. Frequency measured at 2 K for the main $3A_1 + 11E$ vibrational modes inherited from the high-temperature phase are shown in Table 1 in parentheses. Frequencies of most of them exhibit a jump into the high-frequency region under the structural phase transition, however some modes are shifted to lower frequencies (A_1: 476.0 cm^{-1}, E: 159.9 cm^{-1}, TO and LO components in the 350 cm^{-1} region). In our experiment, a large number of additional lines were observed (Table 2). The additional lines arising from the structural phase transition were not analyzed for being TO and LO components since it was not the purpose of the present study. The energy of the vibrational modes corresponding to these additional lines are shown in Table 2 in comparison with literature data for $TbFe_3(BO_3)_4$ and $GdFe_3(BO_3)_4$ crystals.[12]

The majority of the phonon lines did not experience (within the measurement accuracy) any frequency shifts

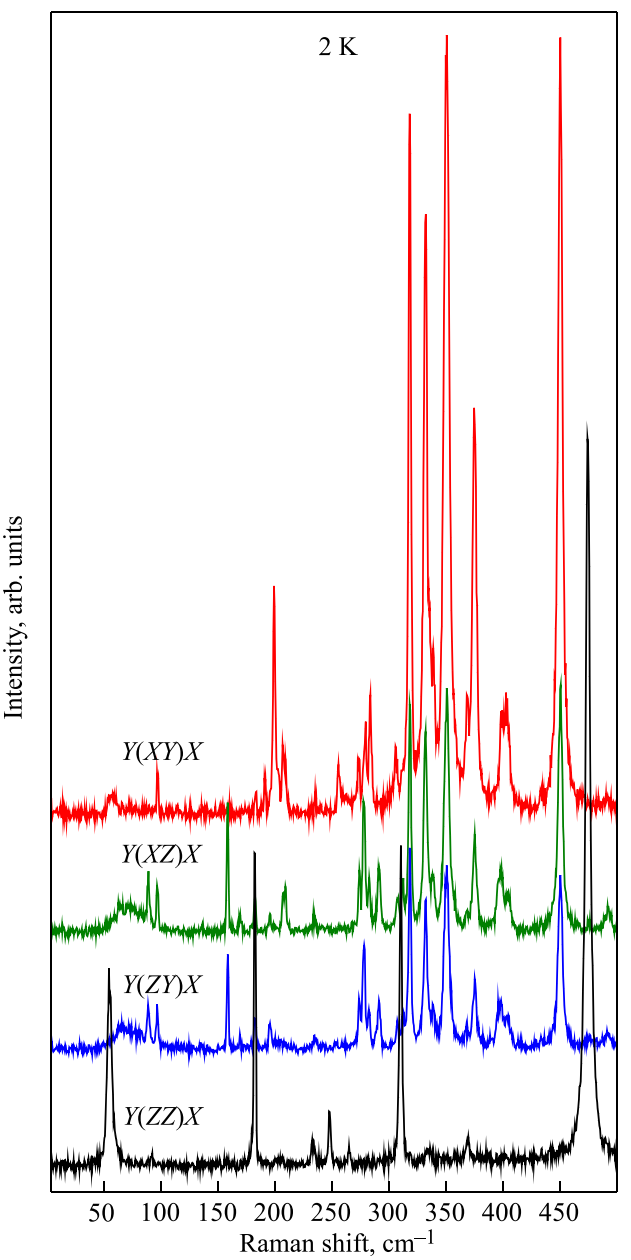

FIG. 3. Raman spectra with different polarizations observed in the region of external vibrational modes of single crystal $TbFe_3(BO_3)_4$ at 2 K; $\lambda_{exc} = 632.8$ nm (30 mW). The spectral resolution is 1.8 cm^{-1}.

TABLE 2. Energy (in cm^{-1}) of the additional vibrational modes observed in the low-temperature phase of single crystal $TbFe_3(BO_3)_4$ at 2 K in comparison with literature data.

$TbFe_3(BO_3)_4$, present study		$TbFe_3(BO_3)_4$, Ref. 12		$GdFe_3(BO_3)_4$, Ref. 12	
A_1	E	A_1	E	A_1	E
55.1	–	54	–	53	101
146.2	114.5	–	–	144	114
203.3	169.5	–	169	203	167
233.4	191.4	232	–	233	–
248.0	195.7	247	–	244	–
265.1	208.1	265	207	263	206
369.2	255.9	368	256	368	254
–	278.4	–	278	–	276
–	283.6	–	282	–	281
–	306.0	–	306	–	305
–	307.5	–	–	–	–
–	312.4	–	311	–	310
–	338.6	–	337	–	337
–	368.5	–	–	–	–
–	375.1	–	375	–	374
–	396.1	–	–	–	–
–	398.9	–	398	–	395
	470.0	–	473	–	472

under the transition to a magnetically ordered state. E_{TO}-modes with frequencies 199 and 256 cm^{-1} were an exception, as shown in Fig. 4. Below T_N they shifted to lower frequencies. Similar behavior has been observed previously for an E_{TO}-mode with frequency 199 cm^{-1} (Ref. 9) and associated with the specific behavior of ε_{ab} below T_N. We checked the response of the "anomalous" lines to an external magnetic field directed along and perpendicular to the third-order axis. Fig. 5 shows the behavior of a Raman spectrum region upon application of a magnetic field along the third-order axis. In order to detect a weak spectrum in a cryostat with a solenoid, a high-power (100 mW) solid-state laser (532 nm) was employed. As can be seen in Fig. 5, the "anomalous" lines at 199 and 256 cm^{-1} and a line at 208 cm^{-1}, which has no apparent anomalies in the temperature behavior, shift to the high-frequency region upon application of an external magnetic field along the c-axis. There were no shift of these and other spectral lines observed in a magnetic field perpendicular to the c-axis.

Upon transition into a magnetically ordered state, in the low-frequency region, a broad band with energy of $\sim$74 cm^{-1} was observed in Raman spectra with XZ- and ZY-components of the scattering tensor (Fig. 3). The spectra obtained in XZ- and YZ-polarizations and in different experimental scattering geometries exhibited identical shape and intensity of the band. The shape of this band and its temperature evolution are shown in Fig. 6. As can be seen, with increasing temperature the shape of this band changes and, at temperatures above T_N up to room temperature, it is observed as a wing of the Rayleigh line (Fig. 6).

It should be noted that at low temperatures, there is an energy peak at 64 cm^{-1} within this band indicated by an arrow in Fig. 6. The half-width of this peak is comparable with those of phonon lines. The inset in Fig. 6 shows fragments of the spectrum in this region obtained at low temperatures at different orientations of the sample, i.e., at $\theta = 45°$ and 90°. As can be seen, the shape of the spectrum in the region of two-magnon scattering does not change. The presence of this peak in the geometry $\theta = 90°$ indicates that the peak is not due to the "leakage" of A_2-mode, which may occur in this frequency range (Table 1). In addition, based on the temperature behavior of the spectrum (Fig. 6), this peak cannot be a phonon line, such as an additional E-mode, since all additional phonon lines are maintained up to the temperature of the structural phase transition. To check whether this peak is related to electron scattering on a Tb^{3+} ion (primary or impurity one located near growth defects[21]), measurements of these spectra were carried out in an external magnetic field parallel and perpendicular to the third-order axis. As was shown by these measurements, neither the shape of the band assigned to two-magnon scattering nor the frequency position of the phonon lines in this range did change upon application of a field in either of the directions. Fig. 7 shows, as an example, the scattering spectra obtained upon application of a field along the third-order axis.

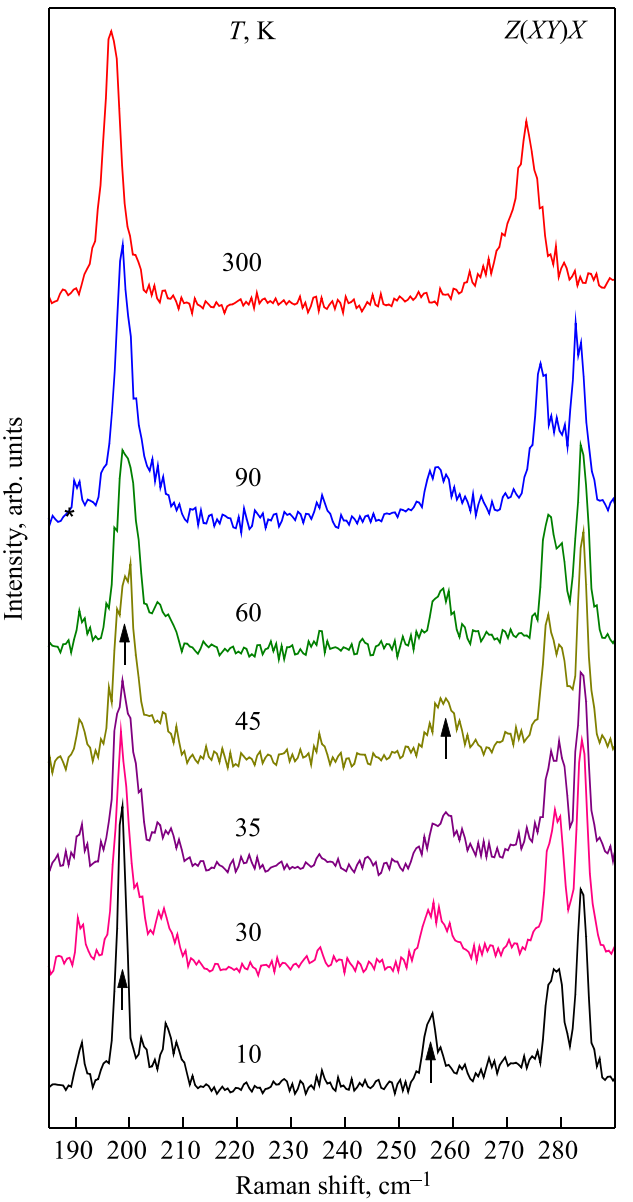

FIG. 4. Temperature behavior of the Raman spectra of single crystal $TbFe_3(BO_3)_4$ in the scattering geometry $Z(XY)X$; $\lambda_{exc} = 632.8$ nm (30 mW). The spectral resolution is 1.8 cm^{-1}.

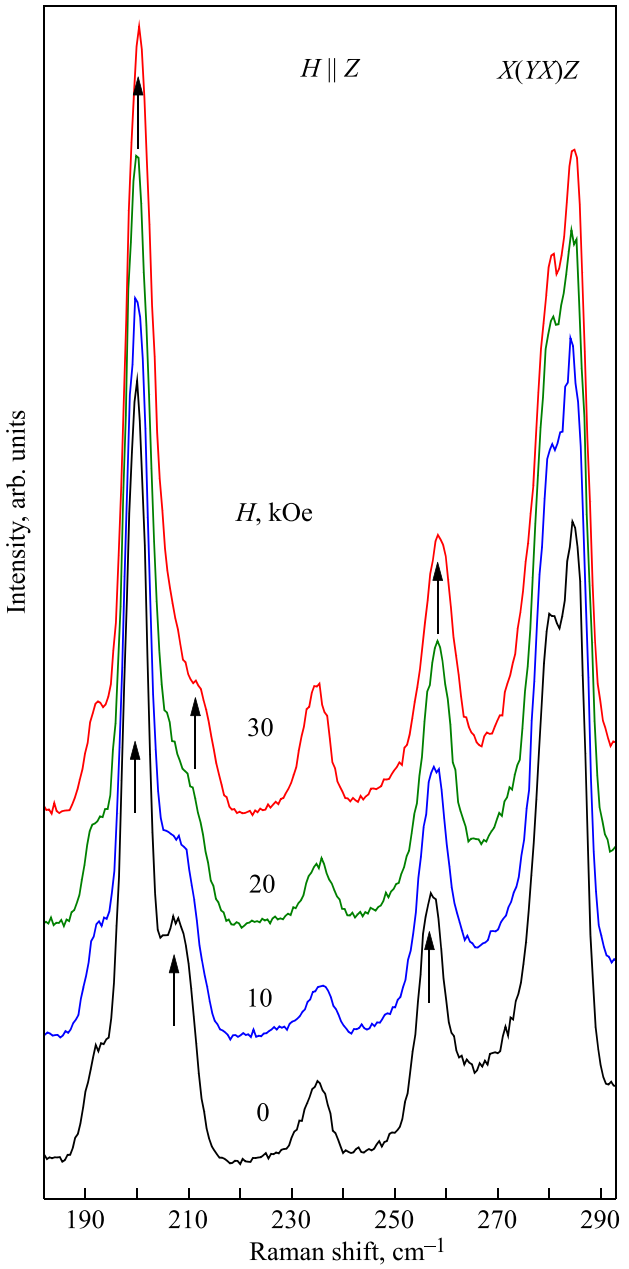

FIG. 5. Behavior of the Raman spectra of single crystal $TbFe_3(BO_3)_4$ in an external magnetic field applied along the third-order axis in the scattering geometry $X(YX)Z$; $\lambda_{exc} = 532$ nm (100 mW). The spectral resolution is 4.0 cm^{-1}.

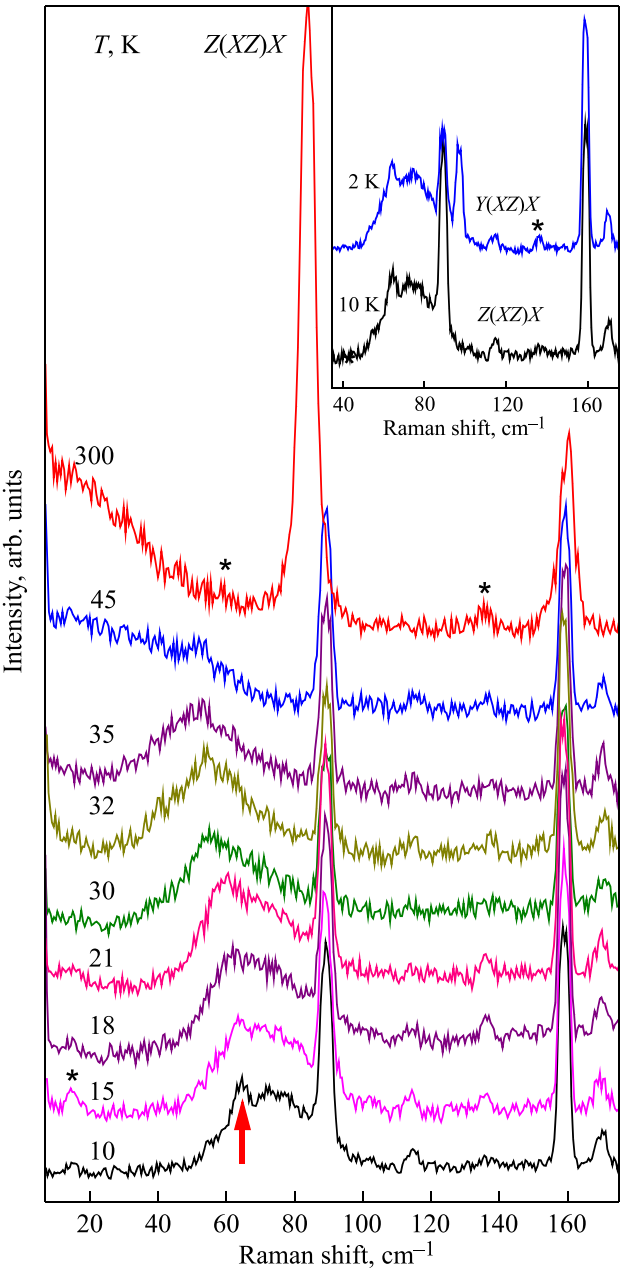

FIG. 6. Temperature behavior of the Raman spectra of single crystal $TbFe_3(BO_3)_4$ in the region of two-magnon scattering in the scattering geometry $Z(XZ)X$; $\lambda_{exc} = 632.8$ nm (30 mW). The spectral resolution is 4.0 cm^{-1}. Plasma lines of the HeNe laser are marked with (*).

Discussion

It is well-known that long-range electrostatic interaction in piezoelectric crystals leads to a splitting of polar E-modes into transverse TO and longitudinal LO modes.[18,20,22] Selecting an appropriate direction of the wave vector **k** and polarization of the incident and scattered radiation allows to observe light scattering on the (LO-TO) components of the E-modes. When a phonon propagates in the basal plane at an angle of 45° to X and Y (Fig. 1), LO and TO components are observed in the light scattering spectrum.

Separation of oscillations is only valid for the most symmetric directions of **k**. Upon changing the direction of **k** vector, an oscillation might change from transverse to longitudinal and vice versa. When the direction of phonon propagation does not coincide with the optical axis, the relative degree of influence of long-range electrostatic and short-range forces should be considered.[20,22] Studies of the scattering spectra on E-oscillations propagating at an angle $\theta \sim 45°$ to the optical axis (Fig. 2) have shown that it is not possible to establish unambiguously, as in the case of α-quartz,[19,20] which forces prevail. When **k** is varied from 0 to 90°, there are two distinct types of behavior. The frequency of the mixed phonon E-mode varies depending on the angle θ between the **k** vector and the crystal c-axis and is determined by the expression: $\omega^2 = \omega^2_{E(TO)}\cos^2\theta + \omega^2_{E(LO)}\sin^2\theta$. For the low-energy E-mode at $\theta = 45°$ a mixed component at 89.5 cm^{-1} was observed (Table 1), the frequency of which followed the above expression. For this mode, the case where the force constants for displacements parallel and perpendicular to the c-axis are significantly different is realized. Another case where the electrostatic forces dominate over the short-range ones was observed for the angular

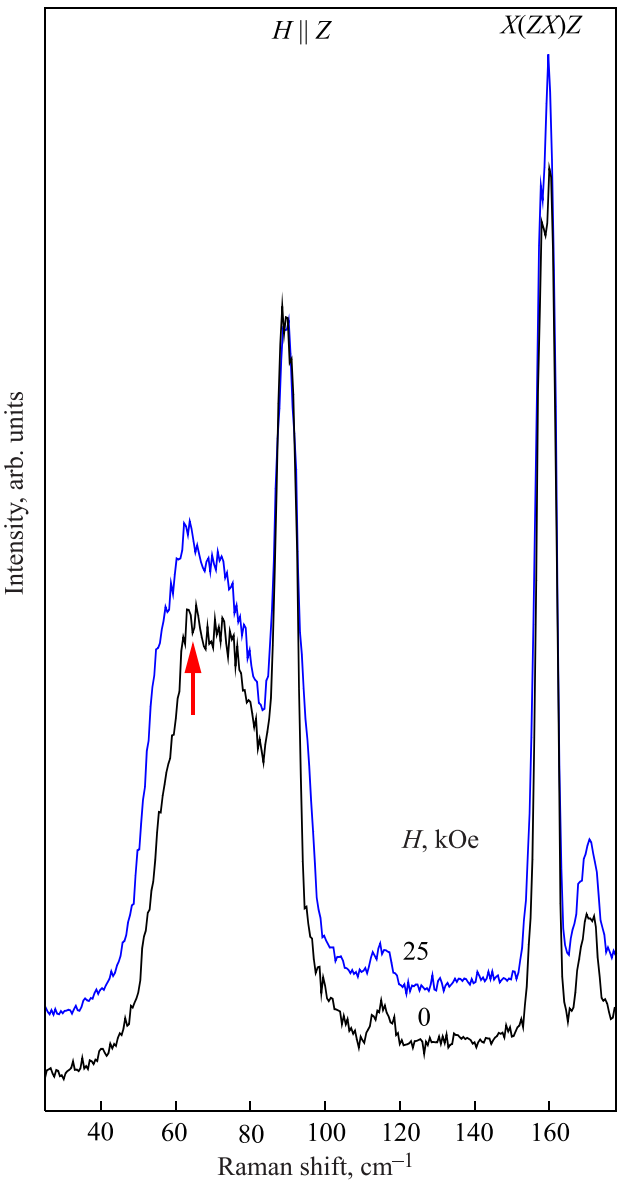

FIG. 7. Behavior of the Raman spectra of single crystal $TbFe_3(BO_3)_4$ in an external magnetic field applied along the third-order axis in the scattering geometry $X(ZX)Z$; $\lambda_{exc} = 532$ nm (100 mW). The spectral resolution is 4.0 cm^{-1}.

dependence of the frequencies of the component pair $\omega_{E(TO)} = 315.4\,cm^{-1}$ and $\omega_{E(LO)} = 330.4$ cm. The component $\omega_{E(TO)} = 315.4\,cm^{-1}$ remains transverse for any angle θ while maintaining the frequency. In the spectra corresponding to the LO components, two lines at 301.4 and 329.4 cm^{-1} (at $\theta = 45°$) with mixed A_2- and E-symmetry were observed (Table 1, Fig. 2).

A large value of splitting can be expected only for the most intensive polar modes since for a single oscillator $\omega_{LO}^2 - \omega_{TO}^2 = \omega_{TO}^2 S/\varepsilon_\infty$, where S is the oscillator strength of the dipole transition. In the frequency range studied in the present paper, the following E-modes exhibited the maximal strength: $\omega_{E(TO)} = 83.7\,cm^{-1}$, $\omega_{E(TO)} = 273.5\,cm^{-1}$, and $\omega_{E(TO)} = 315.4\,cm^{-1}$. The splitting of the remaining modes was small. The splitting of the "anomalous" line at 199 cm^{-1} at room temperature did not exceed 1.2 cm^{-1} and was even less at low temperatures. Thus, the contribution of this mode to the behavior of ε_{ab} as compared to other E-modes is expected to be small.

As follows from the above group-theoretical analysis, new optical vibrational modes $12A_1 + 12A_2 + 24E$ are expected to appear in the studied energy range at $T < T_s$ due to the lowering of symmetry and increasing the volume of the primitive cell. In the low-temperature phase, two non-equivalent positions of the iron ions appear in the unit cell and one of the chains shifts along the c-axis with respect to the other two chains, while the unit cell volume is tripled. The phase transition results in a reduction of the local symmetry of the Tb^{3+}-ion down to C_2. As can be seen from Table 2, at low temperatures a number of additional lines appear due to the lowering of symmetry and cell volume increase.

The temperature behavior of the "anomalous" phonons (Fig. 4) is indicative of spin-phonon coupling. This is further confirmed by their behavior in an external magnetic field **H** $\parallel c$ (Fig. 5). Upon increasing the field, a high-frequency shift and broadening are observed for the lines 199, 208 and 256 cm^{-1}. Two mechanisms of spin-phonon coupling are considered: static and dynamic.

The static mechanism is due to magnetoelastic coupling. According to neutron diffraction studies, the transition to the antiferromagnetic state causes a change in the lattice parameters of $TbFe_3(BO_3)_4$:[7] a decrease in a, a non-monotonous increase in c and a decrease in the cell volume V. The analysis of the exchange interaction pathways indicates[7] that the magnetic interaction of each Fe-spin with the neighboring helical chains is determined by 8 ferromagnetic and 8 antiferromagnetic superexchange pathways with similar lengths but different configurations. It is assumed that the interchain interaction should be transmitted mainly through Fe–O–O–Fe, while the Fe–O–Tb–O–Fe superexchange is less important. Even slight changes in the interatomic distances can lead to changes in the values of the indirect exchange interaction between iron ions. However, no significant changes in the lengths and bond angles at temperatures of 2, 30 and 40 K, which may play a role in changing the magnetic interactions, has been detected.[7]

An increase in force constants upon decreasing the cell volume V should lead to an increase in the vibrational mode frequency. Such a change at $T < T_N$ has been previously observed in the behavior of a "soft" symmetric A_1-mode.[12] The dependence of the magnetostrictive changes in the lattice parameters a, c and cell volume V on the magnetic field applied along the c-axis is small in comparison with the temperature-induced variation of V in the case $H < H_{sf}$.[9] High-frequency shift of the phonon lines in a magnetic field cannot be explained by a small magnetostrictive change in the lattice volume.

In the case of the dynamic mechanism of spin-phonon coupling, there occurs a strong modulation of the exchange coupling constant by certain normal vibrational modes of the lattice. Phonon E-modes involving vibrations of oxygen ions in the basal ab-plane modulate ferromagnetic and antiferromagnetic exchange coupling through the changes in Fe-O lengths and Fe–O–O–Fe angles. The frequency shift of the phonon mode with changing temperature is determined by the spin-correlation function: $\omega = \omega_0 + \lambda\langle S_i S_j\rangle$, where ω is the renormalized phonon frequency, ω_0 is the frequency in the absence of spin-phonon coupling, and λ is the coupling constant.[23,24] The sign of the spin-dependent force constants

of the modulating lattice mode depends on the strength of the ferromagnetic and antiferromagnetic exchange interactions and determines the positive or negative frequency shift of the mode. Thus, the experimentally observed opposite sign of the dependences of the frequency on temperature and external field may be associated with the dynamic mechanism.

In the studies of scattering spectra in rare ferroborates (Re = Y, Er, Tb, Gd, and Nb), a broad band at $\sim 70\,\mathrm{cm}^{-1}$ is commonly observed below the magnetic ordering temperature. This band has been assigned to the two-magnon scattering with generation of a pair of magnons with wave vectors **k** and –**k**.[12] In contrast to the present results, in Ref. 12 a "leakage" of the soft mode A_1 forbidden in the polarizations *XZ* and *YZ* has been observed, which did not allow to reconstruct the contour of the two-magnon scattering. In the present experiment, the leakage of forbidden modes was minimized. Furthermore, both the temperature and field dependences of the two-magnon scattering band indicate that the contributions phonon and electron scattering are not observed there. Thus, the complex shape of the two-magnon scattering band apparently reflects the features of the density of magnon states, dispersion of the magnon branches, and magnon-magnon interaction. Taking into account the tightening of the high-energy tail of the two-magnon band even at low temperatures and the contribution to the shape of the two-magnon scattering by the phonon lineshape $\omega_{E(TO)} = 89.1\,\mathrm{cm}^{-1}$, the magnon energy at the Brillouin zone boundary can be estimated as $E_m \sim 50\,\mathrm{cm}^{-1}$.

Conclusion

On the basis of the conducted temperature studies of Raman scattering in terbium ferroborates, the following conclusions can be drawn. In the high-temperature structural phase, $3A_1 + 11E$ vibrational modes expected in the studied frequency range were observed. The additional phonon lines in the scattering spectrum, found in this study and previously unknown in literature, are related to the observation of LO and TO components of polar phonons. The presence of additional lines in the spectrum of the low-temperature phase is a consequence of the lowering of the crystal symmetry under the structural phase transition and increase in the volume of the primitive cell. The frequency shift of several phonon lines observed upon decreasing temperature below T_N indicates spin-phonon coupling. Upon application of an external magnetic field along the third-order axis, a shift to the high-energy region was observed for a number of phonons, therefore confirming the presence of such a coupling. The study of the two-magnon scattering spectrum showed that the complex shape of the band at low temperature is determined by the magnon dispersion branches, specific features of the density of states, and magnon-magnon interaction. The magnon energy at the Brillouin zone boundary was estimated as $E_m \sim 50\,\mathrm{cm}^{-1}$.

[a)]Email: peschansky@ilt.kharkov.ua

[1]A. K. Zvezdin, S. S. Krotov, A. M. Kadomtseva, G. P. Vorob'ev, Y. F. Popov, A. P. Pyatakov, L. N. Bezmaternykh, and E. A. Popova, Pis'ma Zh. Eksp. Teor. Fiz. **81**, 335 (2005) [JETP Lett. **81**, 272 (2005)].
[2]F. Yen, B. Lorenz, Y. Y. Sun, C. W. Chu, L. N. Bezmaternykh, and A. N. Vasiliev, Phys. Rev. B **73**, 054435 (2006).
[3]A. K. Zvezdin, G. P. Vorob'ev, A. M. Kadomtseva, Yu. F. Popov, A. P. Pyatakov, L. N. Bezmaternykh, A. V. Kuvardin, and E. A. Popova, Pis'ma Zh. Eksp. Teor. Fiz. **83**, 600 (2006) [JETP Lett. **83**, 509 (2006)].
[4]R. P. Chaudhury, F. Yen, B. Lorenz, Y. Y. Sun, L. N. Bezmaternykh, V. L. Temerov, and C. W. Chu, Phys. Rev. B **80**, 104424 (2008).
[5]A. A. Mukhin, G. P. Vorob'ev, V. Yu. Ivanov, A. M. Kadomtseva, A. S. Narizhnaya, A. M. Kuz'menko, Yu. F. Popov, L. N. Bezmaternykh, and I. A. Gudim, Pis'ma Zh. Eksp. Teor. Fiz. **93**, 305 (2011) [JETP Lett. **93**, 275 (2011)].
[6]A. M. Kadomtseva, Yu. F. Popov, G. P. Vorob'ev, A. P. Pyatakov, S. S. Krotov, K. I. Kamilov, V. Yu. Ivanov, A. A. Mukhin, A. K. Zvezdin, A. M. Kuz'menko, L. N. Bezmaternykh, I. A. Gudim, and V. L. Temerov, Fiz. Nizk. Temp. **36**, 640 (2010) [Low Temp. Phys. **36**, 511 (2010)].
[7]C. Ritter, A. Balaev, A. Vorotinov, G. Petrakovskii, D. Velikanov, V. Temerov, and I. Gudim, J. Phys.: Condens. Matter **19**, 196227 (2007).
[8]J. F. Hamman-Borrero, M. Philipp, O. Kataeva, M. V. Zimmermann, J. Geck, R. Klingeler, A. Vasiliev, L. Bezmaternykh, B. Buchner, and C. Hess, Phys. Rev. B **82**, 094411 (2010).
[9]U. Adem, L. Wang, D. Fausti, W. Schottenhamel, P. H. M. van Loosdrecht, A. Vasiliev, L. N. Bezmaternykh, B. Buchner, C. Hess, and R. Kingeler, Phys. Rev. B **82**, 064406 (2010).
[10]A. M. Kuz'menko, A. A. Mukhin, V. Yu. Ivanov, A. M. Kadomtseva, S. P. Lebedev, and L. N. Bezmaternykh, Zh. Eksp. Teor. Fiz. **140**, 131 (2011) [J. Exp. Theor. Phys. **113**, 113 (2011)].
[11]M. I. Pashchenko, V. A. Bedarev, V. I. Kut'ko, L. N. Besmaternykh, and V. L. Temerov, Fiz. Nizk. Temp. **36**, 800 (2010) [Low Temp. Phys. **36**, 638 (2010)].
[12]D. Fausti, A. A. Nugroho, P. H. M. van Loosdreht, S. A. Klimin, and M. N. Popova, Phys. Rev. B **74**, 024403 (2006).
[13]S. Klimin, D. Fausti, A. Meetsma, L. N. Bezmaternykh, P. H. M. van Loosdrecht, and T. M. Palstra, Acta Cryst. B **61**, 481 (2005).
[14]R. Z. Levitin, E. A. Popova, R. M. Chisherbov, A. N. Vasiliev, M. N. Popova, E. P. Chukalina, S. A. Klimin, P. H. M. van Loosdrecht, D. Fausti, and L. N. Bezmaternykh, Pis'ma Zh. Eksp. Teor. Fiz. **79**, 531 (2004) [JETP Lett. **79**, 423 (2004)].
[15]A. A. Demidov, N. P. Kolmakova, L. V. Takunov, and D. V. Volkov, Physica B **398**, 78 (2007).
[16]G. A. Zvyagina, K. R. Zhekov, I. V. Bilych, A. A. Zvyagin, L. N. Bezmaternykh and I. A. Gudim, Fiz. Nizk. Temp. **34**, 1142 (2008) [Low Temp. Phys. **34**, 901 (2008)].
[17]N. Bezmaternykh, V. L. Temerov, L. A. Gudim, and N. A. Stolbovaya, Crystallogr. Rep. **50**(Suppl. 1), 97 (2005).
[18]H. Poulet and J.-P. Mathieu, *Spectres de Vibration et Symetrie des Cristaux* (Cordon and Breach, Paris, 1970).
[19]S. M. Shapiro and J. D. Axe, Phys. Rev. B **6**, 2420 (1972).
[20]W. Hayes and R. Loudon, *Scattering of Light by Crystals* (J. Wiley and Sons, New York, 1978).
[21]V. A. Bedarev, M. I. Paschenko, M. I. Kobets, K. G. Dergachev, V. A. Paschenko, A. N. Bludov, E. N. Khatsko, S. L. Gnatchenko, L. N. Bezmaternykh, and V. L. Temerov, Fiz. Nizk. Temp. **39**, 219 (2013) [Low Temp. Phys. **39**, 167 (2013)].
[22]R. Loudon, Adv. Phys. **13**, 423 (1964).
[23]D. J. Lockwood and M. G. Cottam, J. Appl. Phys. **64**, 5876 (1988).
[24]D. J. Lockwood, Fiz. Nizk. Temp. **28**, 709 (2002) [Low Temp. Phys. **28**, 505 (2002)].

Translated by L. Gardt